Valence engineering of ionic molecular crystals: monovalent-divalent phase diagram for biferrocene-tetracyanoquinodimethane salts

Mochida, Tomoyuki
Funasako, Yusuke
Akasaka, Takahiro
Uruichi, Mikio
Mori, Hatsumi

(Citation)
Crystengcomm,19(11):1449-1453

(Issue Date)
2017-03-21

(Resource Type)
journal article

(Version)
Accepted Manuscript

Journal Name

COMMUNICATION

Valency engineering of ionic molecular crystals: Monovalent–divalent phase diagram for biferrocene–tetracyanoquinodimethane salts†

Received 00th January 20xx,
Accepted 00th January 20xx

DOI: 10.1039/x0xx00000x

www.rsc.org/

Tomoyuki Mochida,*[a] Yusuke Funasako,[a,b] Takahiro Akasaka,[a] Mikio Uruichi,[c] and Hatsumi Mori[d]

The valence state of ionic molecular solids composed of biferrocene derivatives (D) and tetracyanoquinodimethane (TCNQ) derivatives (A), either monovalent ($[D]^+[A_2]^-$) or divalent ($[D]^{2+}[A_2]^{2-}$), can be controlled by changing the redox potentials and molecular volumes of the components.

Sodium chloride (Na^+Cl^-) and magnesium oxide ($Mg^{2+}O^{2-}$) are representative simple ionic compounds, and their valence states are different although they assume the same rock-salt-type structures. The relative stabilities of the monovalent and divalent states in such simple salts depend on the balance between the energies to ionize the components and the coulombic (Madelung) energy in the crystal. In molecular charge-transfer complexes of donor (D) and acceptor (A) molecules, the valence state of the constituent molecules can be tuned by molecular modifications or external stimuli, which has led to various electronic and phase transition phenomena.[1,2] Therefore, we used biferrocene-based molecular salts to search for the transformation between the NaCl- and MgO-type valence states.[3,4] Biferrocene is an electron donor that can produce monocations ($[D]^+$) and dications ($[D]^{2+}$) by oxidation.[5] We discovered previously that a salt of dineopentyl-biferrocene (Np_2-bifc, Fig. 1a (left): R = neopentyl) and fluoro-tetracyanoquinodimethane salt (F_1-TCNQ, Fig. 1a (right): X^1 = F, X^2 = H), with a 1:3 D/A composition, exhibit a phase transition from the monovalent state ($[D]^+[A_3]^-$) to the divalent state ($[D]^{2+}[A_3]^{2-}$) at ~120 K (Fig. 1b).[3] This transition is ascribed to reduced cell volumes upon cooling, which stabilize the divalent state because of the relative increase of the Madelung gain.[3,4] This is a first order transition but occurs over a wide range of temperatures (90–150 K) because of two-phase coexistence.[4a] Control of the phase transition temperature by chemical modification of the components or by application of pressure is possible.[3b,4a]

In molecular charge-transfer complexes composed of donors and acceptors of planar π-conjugated organic molecules, the phase boundary between the neutral ($[D]^0[A]^0$) and ionic ($[D]^+[A]^-$) solids is correlated with the difference of the redox potentials of the donor and acceptor (ΔE).[2a] Similarly, this

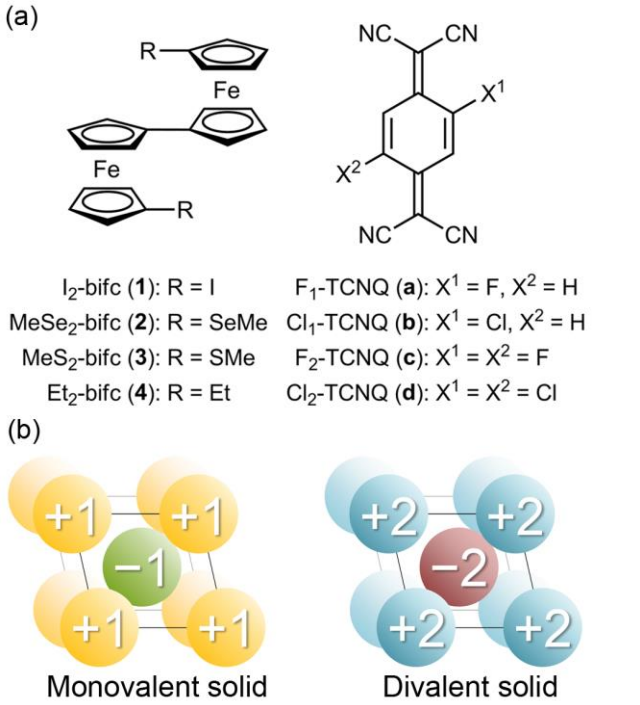

Fig. 1. (a) Chemical formulas of donors (biferrocene derivatives) and acceptors (TCNQ derivatives) used in this study. (b) Schematic illustrations of monovalent salt ($[D]^+[A]_n^-$) and divalent salt ($[D]^{2+}[A_n]^{2-}$) of biferrocenium–TCNQ salts.

[a] *Department of Chemistry, Graduate School of Science, Kobe University, Rokkodai, Nada, Hyogo 657-8501, Japan. E-mail: tmochida@platinum.kobe-u.ac.jp; Fax: +81 78 803 5679; Tel: +81 78 803 5679.*
[b] *Department of Applied Chemistry, Faculty of Engineering, Tokyo University of Science, Yamaguchi, Sanyo-Onoda, Yamaguchi 756-0884, Japan.*
[c] *Institute for Molecular Science, Myodaiji, Okazaki, Aichi 444-8585, Japan.*
[d] *Institute for Solid State Physics, The University of Tokyo, Kashiwanoha, Kashiwa, Chiba 277-8581, Japan*

†Electronic supplementary information (ESI) available: Composition, valence state, intramolecular and intermolecular distances, overlap integrals, and acceptor charges of the salts. Crystallographic parameters, redox potentials of donors and acceptors, unit cell volumes, Ortep drawings of the molecular structures, and crystallographic data. CCDC 1499543–1499550. For ESI and crystallographic data in CIF or other electronic format see DOI:10.1039/x0xx00000x.

Please do not adjust margins

Table 1. Compositions, overlap integral in the dimer, and acceptor charges in **1b–4c**.

	Compound	Intradimer overlap integral[b]	Acceptor charge[c]
Monovalent salts ($[D]^+[A_2]^-$)			
1b[a]	$(I_2\text{-bifc})(Cl_1\text{-TCNQ})_2$		−0.61[d]
1c[a]	$(I_2\text{-bifc})(F_2\text{-TCNQ})_2$	19.3×10^{-3}	−0.51
1d[a]	$(I_2\text{-bifc})(Cl_2\text{-TCNQ})_2$	16.4×10^{-3}	−0.45
2a	$(MeSe_2\text{-bifc})(F_1\text{-TCNQ})_2$		−0.56
2b	$(MeSe_2\text{-bifc})(Cl_1\text{-TCNQ})_2$		−0.57[d]
3a	$(MeS_2\text{-bifc})(F_1\text{-TCNQ})_2$		−0.54
3b	$(MeS_2\text{-bifc})(Cl_1\text{-TCNQ})_2$		−0.40[d]
3d	$(MeS_2\text{-bifc})(Cl_2\text{-TCNQ})_2$	17.5×10^{-3}	−0.53
4b	$(Et_2\text{-bifc})(Cl_1\text{-TCNQ})_2$		−0.58[d]
Divalent salts ($[D]^{2+}[A_2]^{2-}$)			
3c	$(MeS_2\text{-bifc})(F_2\text{-TCNQ})_2$	27.6×10^{-3}	−0.88
4c	$(Et_2\text{-bifc})(F_2\text{-TCNQ})_2$	25.2×10^{-3}	−0.98

[a]Ref. 9. [b]Overlap integrals calculated by the extended Hückel molecular orbital method for salts with non-disordered acceptors (Ref. 13). [c]Estimated from the bond lengths (Ref. 12). [d]The four bonds opposite to the dominant Cl site were used for the estimation.

study aims to investigate the phase boundary between monovalent ($[D]^+[A_n]^-$) and divalent ($[D]^{2+}[A_n]^{2-}$) salts in biferrocene–TCNQ derivatives. For this purpose, we investigated the valence states of the salts composed of R_2-bifc[6,7] (R = I, SeMe, SMe, Et) and X_n-TCNQ[8] (X = F, Cl; n = 1, 2) (Fig. 1b), because the redox potentials of each component can be tuned by changing the substituents (Table S4–S5, ESI†). Vapor diffusion of hexane into chloroform solutions of the donor and acceptor in a 1:2 ratio produced eleven single crystals of charge-transfer salts (**1b**–**4c**, Table 1) in low yields, which were subjected to X-ray crystallographic structure determination. Among them, the crystal structures and valence states of **1b**, **1c**, and **1d** were reported previously.[9]

The structure determination revealed that all of the salts were isomorphous with a 1:2 D/A ratio.[10] The packing diagrams of **3a** and **3c** are shown in Fig. 2. Their compositions differ only in the number of fluorine atoms in the acceptor (F_1-TCNQ (**a**) in **3a** and F_2-TCNQ (**c**) in **3c**), whereas the donors are the same (MeS_2-bifc (**3**)). The fluorine atom of F_1-TCNQ in **3a** is disordered over two sites. In the unit cell, the donors and acceptor dimers are located at the corners and center, respectively, forming a deformed CsCl-like ionic arrangement. There are π–π interactions between the donors and acceptors. Although they have almost identical crystal structures, their valence states are different, as shown below.

The valence state of each salt was determined based on the intramolecular bond lengths, which revealed that **3c** and **4c** were divalent salts ($[D]^{2+}[A_2]^{2-}$), whereas the other nine salts were monovalent salts ($[D]^+[A_2]^-$). The average intramolecular Fe–$Cp_{centroid}$ distances (Cp = cyclopentadienyl ring) in the cations are compared in Fig. S2a and Table S1, ESI†. The distances in the monovalent salts are 1.67–1.69 Å, which are typical values for valence-detrapped biferrocenium monocations ($[D]^+$), while those in the divalent salts are 1.70–1.71 Å, typical values for biferrocenium dications ($[D]^{2+}$).[11] Consistently, the acceptor charges estimated from the intramolecular bond lengths[12] in the monovalent and divalent salts were approximately −0.5 and

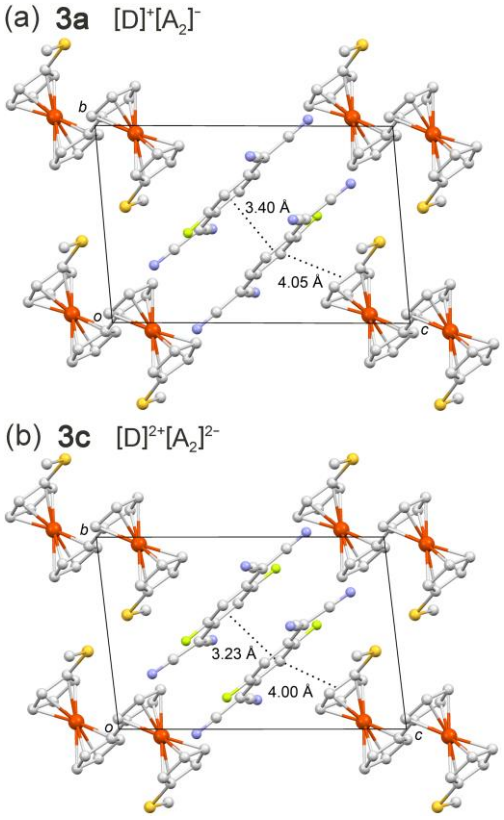

Fig. 2. Packing diagrams of (a) $(MeS_2\text{-bifc})(F_1\text{-TCNQ})_2$ (**3a**, monovalent salt) and (b) $(MeS_2\text{-bifc})(F_2\text{-TCNQ})_2$ (**3c**, divalent salt). The fluorine atom of F_1-TCNQ in **3a** is disordered over two sites. Dotted lines show intermolecular distances.

−1, respectively (Table 1); hence, the dimers are represented as $[A_2]^-$ and $[A_2]^{2-}$, respectively. Another noticeable feature is that the intermolecular distances in the acceptor dimers are shorter in the divalent salts (3.23–3.28 Å) than that in the monovalent salts (3.39–3.51 Å) (Fig. S2b and Table S1, ESI†), as also shown in Fig. 2 (3.23 Å in **3c** and 3.40 Å in **3a**). This feature is consistent with the formation of a diamagnetic dimer in the divalent salts, as expected for TCNQ radical anions. Consistently, the intradimer overlap integrals (S) between the LUMO of the acceptors for $[A_2]^{2-}$ in the divalent salts (**3c**: 27.6×10^{-3}, **4c**: 25.2×10^{-3}) are larger than those for $[A_2]^-$ in the monovalent salts (**1c**, **1d**, and **3d**: $16.4–19.3\times10^{-3}$, Table 1). These data are consistent with each other and unambiguously demonstrate the valence state of each salt.

The valence states determined above were also consistent with the magnetic properties and Raman spectra. The magnetic susceptibilities of **3a**–**c** are shown in Fig. 3. The magnetic moments (χT values) of monovalent salts **3a** and **3b** at 300 K were 0.53 and 0.61 emu K mol^{-1}, respectively, which correspond to one spin in the biferrocenium cation.[11] In contrast, the magnetic moment of the divalent salt **3c** (1.17 emu K mol^{-1}) was approximately twice that for **3a** and **3b**, corresponding to two spins in the biferrocenium dications. Contributions of the acceptor spins are probably suppressed by intermolecular antiferromagnetic interactions.[11] The gradual decrease of the magnetic moment in **3c** below 100 K is characteristic to sulfur-containing

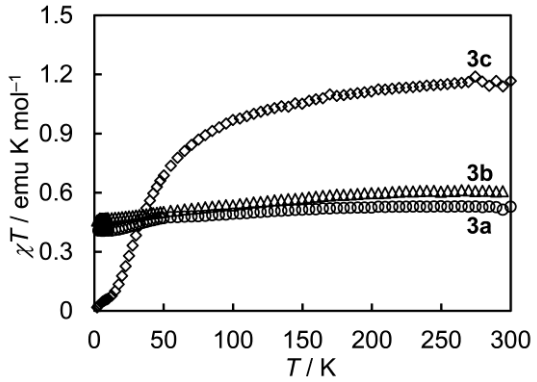

Fig. 3. Temperature dependence of the magnetic susceptibilities of **3a–c** represented in the form of χT vs. T.

biferrocenium dication, which is ascribed to intramolecular strong antiferromagnetic interactions and/or temperature-dependent loss of the orbital contribution.[11] In the Raman spectra, the charge-sensitive C=C stretching modes for the acceptor in monovalent salt **3a** was observed at 1428 cm^{-1}, and those in divalent salt **3c** were observed at 1417 and 1422 cm^{-1}. The former value corresponds to F_1-$TCNQ^{-0.5}$, appearing between those for the F_1-$TCNQ^{-1}$ (1403–1412 cm^{-1}, Li salt) and F_1-$TCNQ^0$ (1460 cm^{-1}), whereas the latter corresponds to F_2-$TCNQ^{-1}$ (1414–1420 cm^{-1}, Li salt).

To find the boundary between the monovalent and divalent salts, the correlation between the valence states and redox potentials of the components was investigated. The relative stabilities of the divalent and monovalent states depend on the free energy change (ΔG) of the following process in the solid state: $[D]^+[A_2]^- \rightarrow [D]^{2+}[A_2]^{2-}$. Redox reactions of each component, viz. $[D]^+ - e^- \rightarrow [D]^{2+}$ and $[A_2]^- + e^- \rightarrow [A_2]^{2-}$, are involved in this reaction, and their electrochemical potentials are related to the second redox potentials of the donor (E_D^2; Tables S4, ESI†) and acceptor dimer (E_{A2}^2), respectively. Therefore, we plotted E_D^2 and E_{A2}^2 for each salt, as shown in Fig. 4a. Although the values of E_{A2}^2 cannot be experimentally determined, they were approximated by adding the value of the intermolecular transfer integral in the dimer (t = −10 S/eV,[13] where $S \approx 2 \times 10^{-3}$, Table 1) to the first redox potential (E_A^1: $[A] + e^- \rightarrow [A]^-$) of the acceptor (Tables S5, ESI†), yielding the relationship $E_{A2}^2 = E_A^1 + 0.2$ (V). Similar electrochemical diagrams, where the first redox potentials E_D^1 and E_A^1 are plotted, are often used to investigate the phase boundary between neutral and ionic organic charge-transfer complexes.[1c] In Fig. 4a, the E_D^2 values for SMe_2-bifc (**3**) and Et_2-bifc (**4**) were almost the same. The differences of the redox potentials ($\Delta E = E_D^2 - E_{A2}^2$) become smaller in the lower left side of the diagram; hence, divalent salts **3c** and **4c** are reasonably located in this region. However, **3d** is a monovalent salt despite its smaller ΔE value than that of **3c** and **4c**. This is due to the larger molecular volume of Cl_2-TCNQ (**d**) than that of F_2-TCNQ (**c**), which results in a smaller Madelung gain of the divalent state. This result indicates that the valence state is governed by both the redox potentials and molecular volumes.

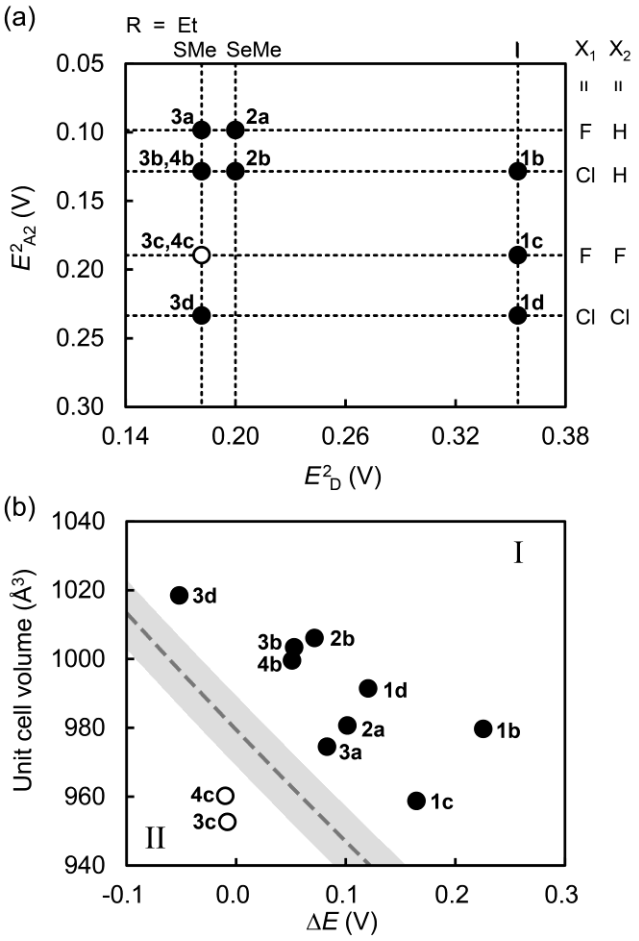

Fig. 4. (a) Monovalent–divalent plot for $(R_2\text{-bifc})(X_n\text{-TCNQ})_2$ based on redox potentials. E_{D2} and $E_{A(Dimer)}$ are redox potentials for $[D]^+ - e^- \rightarrow [D]^{2+}$ and $[A_2]^- + e^- \rightarrow [A_2]^{2-}$, respectively. Closed circles (●) and open circles (○) denote monovalent and divalent salts, respectively. (b) Monovalent–divalent phase diagram based on ΔE (= $E_D^2 - E_{A2}^2$) and unit cell volumes at 173 K. The dotted line represents the calculated phase boundary. The gray area represents the two-phase coexistence region (See text).

To quantitatively examine the effect of the molecular volume, the valence state of each salt is plotted on a ΔE–volume diagram (Fig. 4b), where the vertical axis is the unit cell volume. Divalent salts **3c** and **4c** are located at the lower left region of this diagram. In the monovalent salts, the cell volume of **1c** is smaller than that of **1b** by 20 $Å^3$ because of the volume difference of Cl_1-TCNQ (**b**) and F_2-TCNQ (**c**). However, the cell volumes of divalent salts **3c** and **4c** are approximately 40 $Å^3$ less than that of monovalent salts **3b** and **4b**. The additional 20 $Å^3$ contraction is caused by the stronger Coulomb interaction in the divalent solid. This result is reasonable considering the reduction of the cell volume of $(Np_2\text{-bifc})(F_1\text{-TCNQ})_3$ by 3% at the monovalent–divalent phase transition.[4b] The contraction is also visible in Fig. 2, in which the donor–acceptor distance is shorter in divalent salt **3c** (4.00 Å) than in monovalent salt **3a** (4.05 Å).

Next, we estimated the phase boundary between the monovalent and divalent salts. In the neutral–ionic system, the relative stability of the neutral and ionic solids is simply determined by the balance between the Madelung energy and the energy to ionize each component, hence the phase

boundary is determined by $I_D - E_A = \alpha V$, where $V = (Ze)^2/4\pi\varepsilon d$.[2a] Here, I_D, E_A, α, Z, and d are the ionization potential of the donor, electron affinity of the acceptor, Madelung constant, charge of the ion (= 1), and intermolecular distance, respectively. In that system, $\Delta E + \Delta G = \alpha V$ holds with respect to ΔE (= $E_D^1 - E_A^1$), where ΔG is the solvation energy in solution (3.9 eV for planar organic π-conjugated molecules[2a]). Based on these relationships, $\Delta E+\Delta G = 3\alpha V$ is derived for the present system by considering the difference of Z. The calculated phase boundary using this formula, assuming α = 1.763 and ΔG = 8.86 eV, is shown by a dotted line in Fig. 4b. The value of α for the CsCl structure is 1.763. The value of ΔG for this system cannot be determined experimentally; however, a value within 8.86±0.03 reproduced the valence states in the diagram. On the other hand, if we simply assume that the solvation energy is proportional to $-Z^2/r$ (according to the Born equation, where r is the ionic radius), then the value of ΔG for the biferrocene system is estimated to be 9.3 eV based on ΔG = 3.9 eV for planar organic molecules. Therefore, the assumed ΔG value seems to be reasonable. The phase boundary has a width of approximately 20 Å^3, as shown by the shaded area in Fig. 4b, owing to the volume difference between the monovalent and divalent salts (~20 Å^3). In the shaded area, two-phase coexistence is expected to occur. This consideration is supported by the two-phase coexistence in the monovalent–divalent phase transition of (Np_2-bifc)(F_1-TCNQ)$_3$.[4a] This is a first order transition but occurs over a wide range of temperatures (90–150 K) owing to the large volume difference of the two phases.

In conclusion, our systematic investigation of the isomorphous crystals of biferrocene–TCNQ salts revealed that their valence states, either monovalent ($[D]^+[A_2]^-$) or divalent ($[D]^{2+}[A_2]^{2-}$), are reasonably understood in terms of the redox potentials and volumes of the constituent molecules. In the neutral–ionic system composed of planar π-conjugated molecules, the role of the molecular volume is less significant because these are essentially one-dimensional systems.[2a] In contrast, the volume effect is essential in the biferrocene–TCNQ salts because of the three-dimensional nature of the structure and interaction. Based on the phase diagram, monovalent salts located close to the phase boundary is expected to exhibit a transition to the divalent state at low temperatures or high pressures. Indeed, Raman spectroscopy revealed that **1c** and **3a** exhibit a phase transition to the divalent state at low temperatures and high pressures.[14] This study demonstrates that valence control of ionic molecular solids is possible from a crystal engineering approach.

This work was supported financially by KAKENHI (grant numbers 16H04132 and 18028022).

Notes and references

1 (*a*) *Organic Conductors, Superconductors and Magnets: From Synthesis to Molecular Electronics,* ed. L. Ouahab, E.Yagubskii, Springer, 2004; (*b*) *Conducting and magnetic Organometallic Molecular Materials, Topics in Organometallic Chemistry, Vol. 27*, ed. M. Fourmigué, L. Ouahab, Springer, 2009; (*c*) G. Saito and Y. Yoshida, *Bull. Chem. Soc. Jpn.,* 2007, **80**, 1–137.

2 (*a*) J. B. Torrance, J. E. Vazquez, J. J. Mayerle and V. Y. Lee, *Phys. Rev. Lett.,* 1981, **46**, 253–257; (*b*) S. Horiuchi, Y. Okimoto, R. Kumai and Y. Tokura, *Science*, 2003, **299**, 229; (*c*) E. Collet, M. -H. Lemée-Cailleau, M. B. -L. Cointe, H. Cailleau, M. Wulff, T. Luty, S. Koshihara, M. Meyer, L. Toupet, P. Rabiller and S. Techert, *Science*, 2003, **300**, 612–615

3 (a) T. Mochida, Y. Funasako, K. Takazawa, M. Takahashi, M. M. Matsushita, T. Sugawara, *Chem. Commun.*, 2014, **50**, 5473–5475; (b) T. Mochida, K. Takazawa, M. Takahashi, M. Takeda, Y. Nishio, M. Sato, K. Kajita, H. Mori, M. M. Matsushita, T. Sugawara, *J. Phys. Soc. Jpn.*, 2005, **74**, 2214–2216.

4 (*a*) M. Uruichi, Y. Yue, K. Yakushi and T. Mochida, *J. Phys. Soc. Jpn.,* 2007, **76**, 124707/1–6; (b) M. Uruichi, K. Yakushi and T. Mochida, *J. Low Temp. Phys*., 2006, **142**, 655–658; (*c*) M. Sato, Y. Nishio, T. Mochida and K. Kajita, *J. Phys.: Conf. Ser*., 2009, **150**, 042173/1–4; (*d*) H. Shimahara, *J. Phys. Soc. Jpn.*, 2005, **74**, 823–826.

5 (*a*) D. O. Cowan, R. L. Collins and F. J. Kaufman, *J. Phys. Chem.,* 1971, **75**, 2025−2030; (*b*) D. N. Hendrickson, S. M. Oh, T. -Y. Dong, T. Kambara, M. J. Cohn and M. F. Moore, *Comments Inorg. Chem.*, 1985, **4**, 329–349; (c) S. Nakashima, Y. Masuda, I. Motoyama and H. Sano, *Bull. Chem. Soc. Jpn*., 1987, **60**, 1673–1680.

6 (a) R. F. Kover, M. D. Rausch and H. Rosenberg, *Organomet. Chem. Synth*., 1971, **1**, 173–181; (b) T. -Y. Dong, C. -K. Chang, S. -H. Lee, L. -L. Lai, M. Y. -N. Chiang and K. -J. Lin, *Organometallics*, 1997, **16**, 5816–5825; (c) S. Iijima, R. Sada, I. Motoyama and H. Sano, *Bull. Chem. Soc. Jpn.*, 1981, **54**, 1375–1379.

7 1′,1‴-Bis(methylseleno)-1,1′′-biferrocene (**2**) was synthesized as follows. Under nitrogen atmosphere, *n*-butyllithium (1.83 mL, 2.85 mmol; 1.56 M in hexane) was slowly added to a solution of 1′,1‴-dibromo-1,1′′-biferrocene (600 mg, 1.14 mmol) in tetrahydrofuran (40 mL) at −30 °C. After stirring for 30 min, dimethyl diselenide (0.27 mL, 2.85 mmol) was added with stirring, and the solution was allowed to warm to room temperature. After stirring overnight, the reaction was quenched with a small amount of water. After the usual workup, the product was recrystallized from hexane (527 mg, yield 83%). HRMS(ES$^+$): *m/z* calcd for $[C_{22}H_{22}Fe_2Se_2]^+$ 557.8751, found 557.8751.

8 T. Mochida, T. Hasegawa, S. Kagoshima, S. Sugiura and Y. Iwasa, *Synth. Met*., 1997, **86**, 1797–1798.

9 T. Mochida, Y. Funasako, S. Yamazaki and H. Mori, *Eur. J. Inorg. Chem*., 2014, **24**, 3920–3926.

10 X-ray data were collected using Mo(*Kα*) radiation on a Bruker APEX II diffractometer. Crystallographic data and ORTEP diagrams are shown in Tables S1–S2 and Fig. S1 (ESI†), respectively. F_1- and Cl_1-TCNQ in these salts exhibited two-fold disorder of the halogen atoms with occupancies of 0.34:0.66–0.50:0.50. The terminal methyl groups of the substituents in Et_2-bifc were disordered over two sites with occupancies of 0.34:0.66 (**4b**) and 0.45:0.55 (**4c**). Unit cell volumes of **3a**–**c** at different temperatures are shown in Tables S6, ESI†.

11 (a) T. Mochida, T. Akasaka, Y. Funasako, Y. Nishio and H. Mori, *Cryst. Growth Des*., 2013, **13**, 4460–4468; (b) T. Mochida, E. Nagabuchi, M. Takahashi and H. Mori, *Chem. Commun.*, 2014, **50**, 2481–2483.

12 T. J. Kistenmacher, T. J. Emage, A. N. Bloch and D. O. Cowan, *Acta Crystallogr.*, *Sect B*, 1982, **38**, 1193−1199.

13 T. Mori, A. Kobayashi, Y. Sasaki, H. Kobayashi, G. Saito and H. Inokuchi, *Bull. Chem. Soc. Jpn.*, 1984, **57**, 627−633.

14 M. Uruichi and K. Yakushi, unpublished results.

Table of contents entry

The valence state of ionic molecular solids composed of biferrocene derivatives (D) and tetracyanoquinodimethane (TCNQ) derivatives (A), either monovalent ($[D]^{+}[A_2]^{-}$) or divalent ($[D]^{2+}[A_2]^{2-}$), can be controlled by changing the redox potentials and molecular volumes of the components.

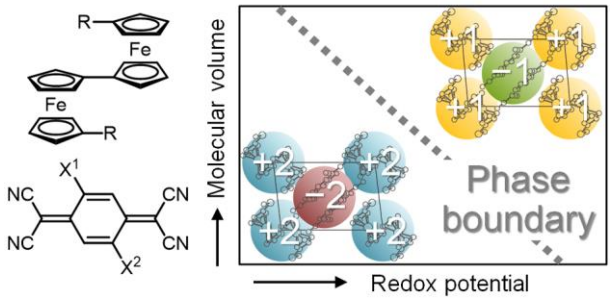

Electronic Supporting Information

Valence engineering of ionic molecular crystals: Monovalent–divalent phase diagram for biferrocene–tetracyanoquinodimethane salts

Tomoyuki Mochida,*[a] Yusuke Funasako,[a,b] Takahiro Akasaka,[a] Mikio Uruichi[c] and Hatsumi Mori[d]

[a]*Department of Chemistry, Graduate School of Science, Kobe University, Rokkodai, Nada, Hyogo 657-8501, Japan. E-mail: tmochida@platinum.kobe-u.ac.jp; Fax: +81 78 803 5679; Tel: +81 78 803 5679.*

[b]*Department of Applied Chemistry, Faculty of Engineering, Tokyo University of Science, Yamaguchi, Sanyo-Onoda, Yamaguchi 756-0884, Japan*

[c]*Institute for Molecular Science, Myodaiji, Okazaki, Aichi 444-8585, Japan*

[d]*Institute for Solid State Physics, The University of Tokyo, Kashiwanoha, Kashiwa, Chiba 277-8581, Japan*

Table S1. Composition, valence state, intramolecular and intermolecular distances, overlap integral in the dimer, and acceptor charges in **1b**–**4c**.

Compound		Valence state	$Fe–Cp_{centroid}$/ Å	Intradimer A···A distances[a] / Å (S^b)	Interdimer A···A distances[a] / Å (S^b)	Acceptor charge[c]
1b[d]	$(I_2\text{-bifc})(Cl_1\text{-TCNQ})_2$	$[D]^+[A_2]^-$	1.686, 1.679	3.451	7.049	–0.61[e]
1c[d]	$(I_2\text{-bifc})(F_2\text{-TCNQ})_2$	$[D]^+[A_2]^-$	1.683, 1.673	3.406 (19.3×10^{-3})	7.010 (5.19×10^{-3})	–0.51
1d[d]	$(I_2\text{-bifc})(Cl_2\text{-TCNQ})_2$	$[D]^+[A_2]^-$	1.685, 1.677	3.506 (16.4×10^{-3})	7.114 (4.61×10^{-3})	–0.45
2a	$(MeSe_2\text{-bifc})(F_1\text{-TCNQ})_2$	$[D]^+[A_2]^-$	1.678, 1.674	3.404	7.090	–0.56
2b	$(MeSe_2\text{-bifc})(Cl_1\text{-TCNQ})_2$	$[D]^+[A_2]^-$	1.680, 1.671	3.414	7.207	–0.57[e]
3a	$(MeS_2\text{-bifc})(F_1\text{-TCNQ})_2$	$[D]^+[A_2]^-$	1.680, 1.674	3.394	6.973	–0.54
3b	$(MeS_2\text{-bifc})(Cl_1\text{-TCNQ})_2$	$[D]^+[A_2]^-$	1.681, 1.671	3.408	7.083	–0.40[e]
3c	$(MeS_2\text{-bifc})(F_2\text{-TCNQ})_2$	$[D]^{2+}[A_2]^{2-}$	1.709, 1.701	3.232 (27.6×10^{-3})	7.069 (4.34×10^{-3})	–0.88
3d	$(MeS_2\text{-bifc})(Cl_2\text{-TCNQ})_2$	$[D]^+[A_2]^-$	1.684, 1.678	3.500 (17.5×10^{-3})	7.253 (7.60×10^{-3})	–0.53
4b	$(Et_2\text{-bifc})(Cl_1\text{-TCNQ})_2$	$[D]^+[A_2]^-$	1.689, 1.673	3.421	6.962	–0.58[e]
4c	$(Et_2\text{-bifc})(F_2\text{-TCNQ})_2$	$[D]^{2+}[A_2]^{2-}$	1.712, 1.707	3.283 (25.2×10^{-2})	7.074 (3.38×10^{-3})	–0.98

[a]Centroid–centroid distances. [b]Overlap integrals calculated by the extended Hückel molecular orbital method for salts with non-disordered acceptors (Ref. 13). [c]Estimated from the bond lengths (Ref. 12). [d]Ref. 9. [e]The four bonds opposite to the dominant Cl site were used for the estimation.

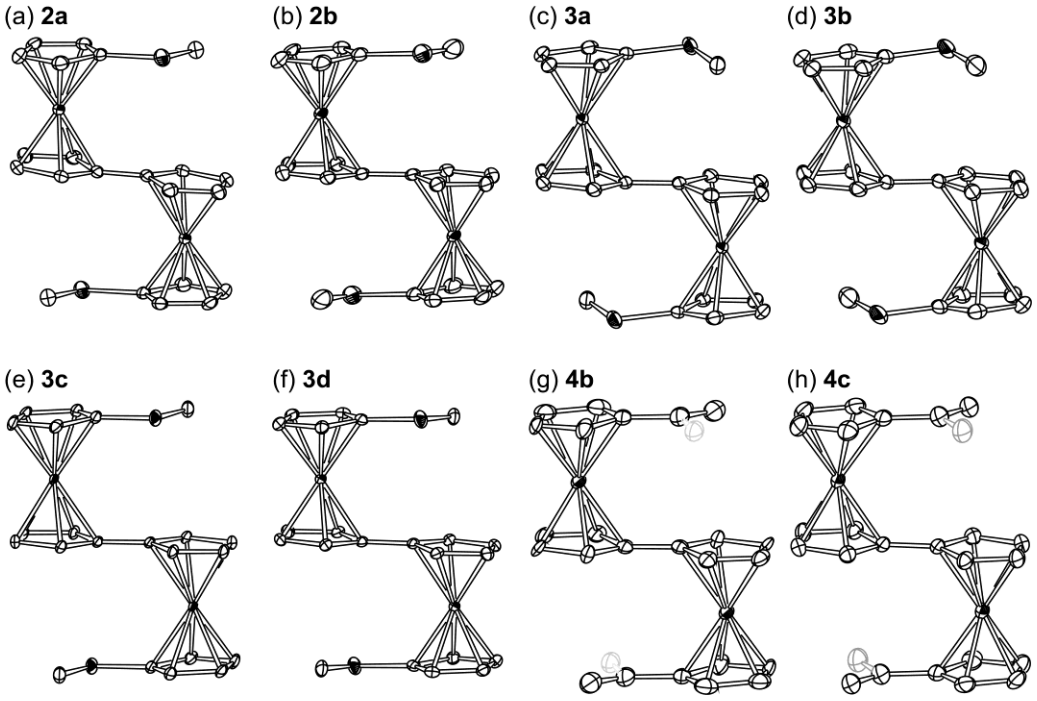

Fig. S1. Ortep drawings of the molecular structures of the cation in each salt. One of the disordered moieties in **4b** and **4c** are displayed in gray. Hydrogen atoms have been omitted for clarity.

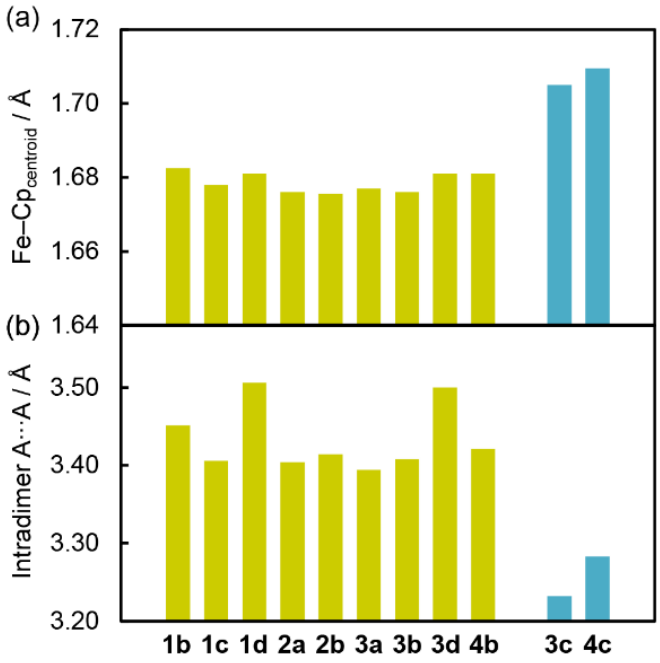

Fig. S2. (a) Average Fe–Cp$_{centroid}$ distances in the cation and (b) intermolecular distances (centroid–centroid) in the acceptor dimers in monovalent salts (yellow) and divalent salts (blue).

Table S2. Crystallographic Parameters.

	2a	**2b**	**3a**	**3b**
Empirical formula	C46H28F2Fe2N8Se2	C46H28Cl2Fe2N8Se2	C46H28F2Fe2N8S2	C46H28Cl2Fe2N8S2
Formula weight	1000.38	1033.28	906.58	939.48
Crystal system	Triclinic	Triclinic	Triclinic	Triclinic
a / Å	8.7623(9)	8.7700(12)	8.7638(7)	8.8205(8)
b / Å	9.1250(10)	9.2110(12)	9.0088(7)	9.0902(8)
c / Å	13.4315(14)	13.5822(19)	13.4894(11)	13.6352(13)
α / deg	90.012(2)	89.993(3)	90.103(2)	90.168(2)
β / deg	106.064(2)	75.599(3)	106.079(2)	104.444(2)
γ / deg	107.409(2)	71.823(3)	107.018(2)	107.949(2)
V / Å	980.68(18)	1006.1(2)	974.55(13)	1003.40(16)
Space group	*P*–1	*P*–1	*P*–1	*P*–1
Z value	1	1	1	1
D_{calc} / g cm^{-3}	1.694	1.705	1.545	1.555
F (000)	498	514	462	478
No. of reflections	7290	7433	7228	7478
No. of observations	4807	4946	4769	4941
Parameters	282	282	282	282
Temperature / K	173	173	173	173
R_1[a],R_w[b] ($I > 2\sigma$)	0.0410, 0.1039	0.0599, 0.1526	0.0438, 0.1068	0.0664, 0.1705
R_1[a],R_w[b] (all data)	0.0603, 0.1132	0.1001, 0.1787	0.0585, 0.1143	0.0805, 0.1809
Goodness of fit	1.052	1.059	1.048	1.046

[a]$R_1 = \Sigma||F_o| - |F_c|| / \Sigma|F_o|$; [b]$R_w = [\Sigma w (F_o^2 - F_c^2)^2 / \Sigma w (F_o^2)^2]^{1/2}$

Table S3. Crystallographic Parameters.

	3c	**3d**	**4b**	**4c**
Empirical formula	C46H26F4Fe2N8S2	C46H26Cl4Fe2N8S2	C48H32Cl2Fe2N8	C48H30F4Fe2N8
Formula weight	942.57	1008.37	903.42	906.51
Crystal system	Triclinic	Triclinic	Triclinic	Triclinic
a / Å	8.7754(10)	8.8175(12)	8.654(3)	8.7951(13)
b / Å	9.0556(11)	9.1617(12)	9.111(3)	9.1673(13)
c / Å	13.2444(16)	13.8108(18)	13.738(4)	13.4002(18)
α / deg	91.068(2)	90.540(2)	89.225(5)	92.358(12)
β / deg	105.733(2)	103.988(2)	75.034(5)	104.633(12)
γ / deg	108.766(2)	109.5500(10)	73.200(5)	109.317(11)
V / Å	952.7(2)	1015.2(2)	999.6(5)	977.3(2)
Space group	*P*–1	*P*–1	*P*–1	*P*–1
Z value	1	1	1	1
D_{calc} / g cm^{-3}	1.643	1.649	1.501	1.540
F (000)	478	510	462	462
No. of reflections	6775	4872	4231	4780
No. of observations	4605	3535	3346	4487
Parameters	281	281	290	284
Temperature / K	173	150	173	296
R_1[a],R_w[b] ($I > 2\sigma$)	0.0465, 0.1149	0.0373, 0.0839	0.0783, 0.1838	0.0314, 0.0768
R_1[a],R_w[b] (all data)	0.0600, 0.1227	0.0500, 0.0911	0.1437, 0.2199	0.0433, 0.0811
Goodness of fit	1.036	1.027	0.969	1.020

[a] $R_1 = \Sigma|| F_o | - |F_c || / \Sigma| F_o |$; [b] $R_w = [\Sigma w (F_o^2 - F_c^2)^2 / \Sigma w (F_o^2)^2]^{1/2}$

Table S4. Redox potentials of donors (in V vs. $[FeCp_2]^{0/+}$) measured in CH_2Cl_2 solutions containing Bu_4NClO_4 (0.1 mol dm^{-3}) as the supporting electrolyte (scan rate 0.1 Vs^{-1}).

	Bifc$^{+/0}$			Bifc$^{2+/+}$			
Compound	E_p^a	E_p^c	$E_{1/2}^1$	E_p^a	E_p^c	$E_{1/2}^2$	$\Delta E_{1/2}$
I_2-bifc (**1**)	0.09	0.02	0.06	0.40	0.31	0.35	0.30
$SeMe_2$-Bifc (**2**)	–0.04	–0.11	–0.08	0.23	0.17	0.20	0.28
SMe_2-Bifc (**3**)	–0.06	–0.15	–0.11	0.23	0.13	0.18	0.29
Et_2-bifc (**4**)	–0.13	–0.20	–0.16	0.22	0.14	0.18	0.34

Table S5. Redox potentials of acceptors (in V vs. $[FeCp_2]^{0/+}$) measured in CH_2Cl_2 solutions containing Bu_4NClO_4 (0.1 mol dm^{-3}) as the supporting electrolyte (scan rate 0.1 Vs^{-1}).

	$[A]^{-/0}$			$[A]^{2-/-}$			
Compound	E_p^a	E_p^c	$E_{1/2}^1$	E_p^a	E_p^c	$E_{1/2}^2$	$\Delta E_{1/2}$
F_1-TCNQ (**a**)	–0.06	–0.14	–0.10	–0.60	–0.74	–0.67	0.57
Cl_1-TCNQ (**b**)	–0.04	–0.11	–0.07	–0.55	–0.66	–0.61	0.53
F_2-TCNQ (**c**)	0.03	–0.05	–0.01	–0.51	–0.63	–0.57	0.56
Cl_2-TCNQ (**d**)	0.07	0.00	0.03	–0.43	–0.55	–0.49	0.52

Table S6. Unit cell volumes of **3a**–**c** at different temperatures.

compound	V (293 K) / Å^3	V (173 K) / Å^3	ΔV/ Å^3
3a	992.3	974.6	–17.8 (–1.8%)
3b	1026.2	1003.4	–22.8 (–2.2%)
3c	969.3	952.7	–16.6 (–1.7%)

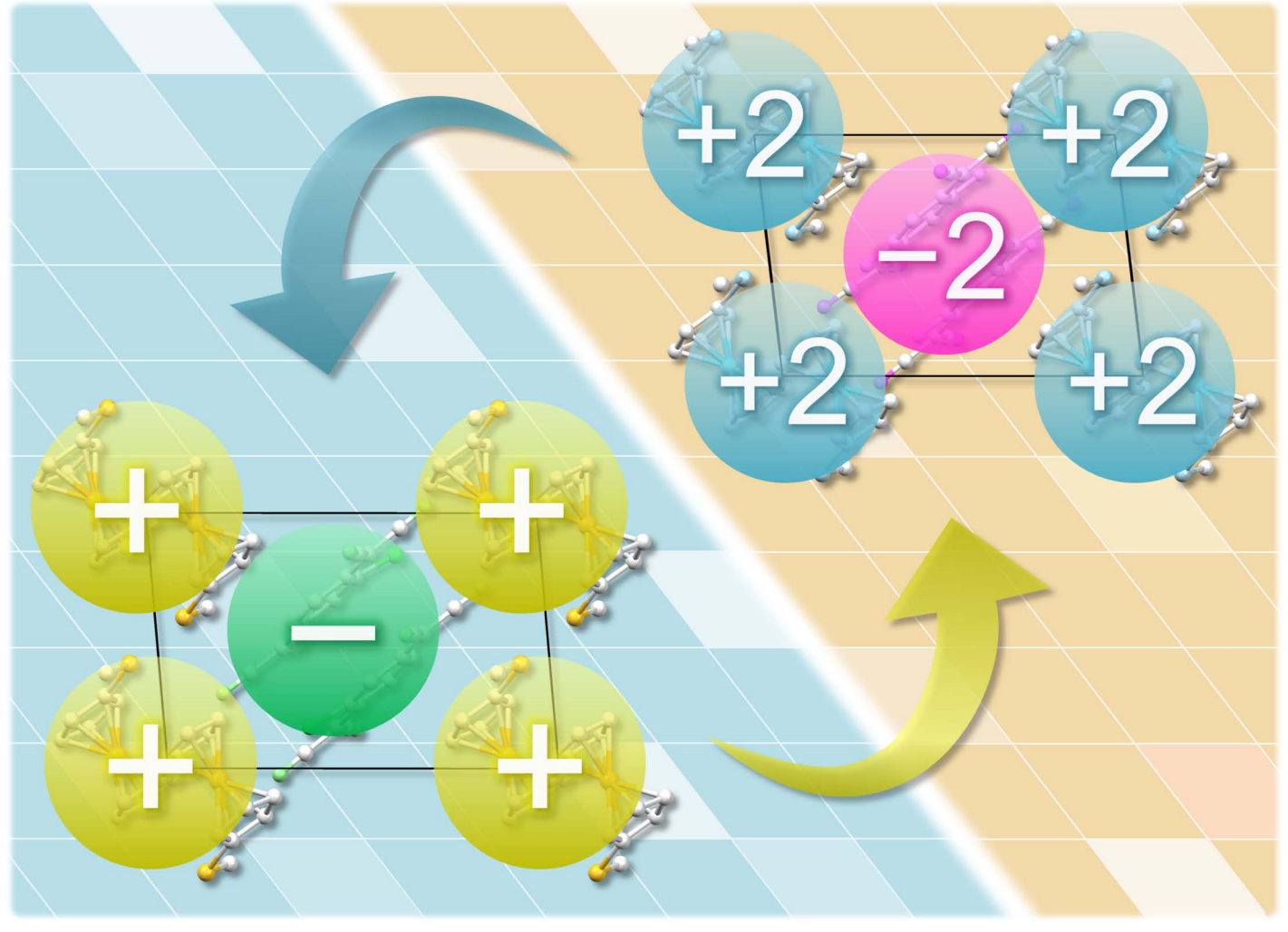
+2
+2
−2
+2
+2
+
+
−
+
+